Rev.Adv.Mater.Sci. 25 (2010) 67-73

STRUCTURE AND PROPERTIES OF Ni-BASED AMORPHOUS RIBBONS CONSOLIDATED BY HIGH PRESSURE TORSION

G. Korznikova[1], T. Czeppe[2] and A. Korznikov[1]

[1]Institute of Metals Superplasticity Problems, Russian Academy of Sciences, Khalturin st. 39, 450001, Ufa, Russia
[2]Institute of Metallurgy and Materials Sciences, Polish Academy of Sciences, Reymonta 25 St. 30-059 Krakow, Poland

Received: November 18, 2005

Abstract. Two Ni-Ti-Zr -based amorphous ribbons of compositions $Ni_{56}Cu_2Zr_{18}Ti_{16}Al_3Si_5$ and $Ni_{36}Cu_{23}Zr_{18}Ti_{14}Al_5Si_4$ were prepared by melt-spun techniques. Such pieces of ribbons were consolidated under the same conditions on Bridgman anvils using a pressure of 6 GPa at room temperature. Samples in the form of discs, 6–7 times thicker than the ribbons and about 10 mm in diameter, were produced by this high pressure torsion (HTP) process. XRD and TEM showed that the microstructure of the samples was dependent on the composition. The sample with the low Cu content revealed higher glass forming ability, thermal stability, tensile strength, Young's modulus, and hardness but partially crystallized during cold consolidation, while the sample with the high Cu content preserved the amorphous state. These results suggest that the thermal stability is not an indicator for retaining the amorphous phase in the HPT process.

1. INTRODUCTION

Bulk metal glasses are relatively novel materials and show outstanding mechanical properties [1]. In particular, they are characterized by a low Young's modulus and high yield stress. Recently researchers succeeded in synthesizing bulk samples in the form of ingots with a few millimetres in thickness by means of special careful casting techniques for selected alloy compositions characterized by extremely high glass-forming ability [2]. However rapid solidification technique on fast rotating metallic wheel enables the production of ribbons for a wide range of alloy compositions [3]. The thickness of ribbons is typically 10-50 micrometer.

Bulk metal glasses can also be prepared by consolidation of ribbons using techniques preventing crystallization. For example the high pressure torsion (HTP) method was successfully applied for consolidation of powder or milled powder samples [4]. In the case of amorphous materials the method was applied to produce massive samples from the melt-spun ribbons by consolidation at room temperature [5-7]. This application is especially interesting for the amorphous alloys since it is relatively easy to fabricate them by melt spinning methods. However, it remains difficult to prepare bulk amor-

Corresponding author: G. Korznikova, e-mail: korznikova@anrb.ru

phous samples. The large strains occurring in the HPT process may induce crystallization in the amorphous matrix [5-7]. It is considered that the crystallization is athermal in nature [8]. The crystallization induced by HPT reveals a radial dependence from the rotation axis and on the range of the accumulated shear strain. It also affects the path of the further, thermal crystallization of the remaining amorphous phase [7]. The present work investiagtes the microstructure and properties of the Ni-Ti-Zr based amorphous ribbons consolidated by HPT at room temperature in comparison with the properties of the as quenched ribbons.

2. EXPERIMENTAL

Two alloys of the compositions $Ni_{56}Cu_2Zr_{18}Ti_{16}Al_3Si_5$ (Ni-1), and $Ni_{36}Cu_{23}Zr_{18}Ti_{14}Al_5Si_4$ (Ni-2) were made from pure elements of 3N and 4N purity using the levitation method under an argon atmosphere. Ribbons were produced by melt spinning in He atmosphere using quartz crucibles. The melt was ejected onto a rotating CuCoBe wheel of 20 cm in diameter with a velocity of 19 m/s. The cold consolidation of the ribbons was performed in the following way: the ribbons were cut into 10–12 mm pieces and six or four parts of each were consolidated under quasi-hydrostatic conditions. Bridgman anvils of 8 mm in diameter, a pressure of 6 GPa and two full turns were used in the HPT process. The amount of strain during the HPT process was estimated by the following expression:

$$e = \ln\left(1+\left(\frac{\varphi * R}{h_{iR}}\right)^2\right)^{\frac{1}{2}}, \qquad (1)$$

where h_{iR} is the height of the sample after processing at a distance R from the center, φ – is the rotation angle of the mobile anvil in radians.

Transmission and scanning electron microscopy were performed using a JEM 2000EX and JSM 840 microscopes respectively. The cross sections of HPT samples were analyzed with Axiovert optical microscope. Phase analysis was performed with a Philips PW 1830 diffractometer using Cu Kα radiation. For thermal analysis DSC Q1000 and SDT Q600 (TA Instruments) were used. The specimens for the bending tests were spark–cut from the HPT samples at a distance of 1 mm from the center of the discs and subsequently grinded and polished to final dimensions 1.5 x 0.2 x 6 mm. Three point bending tests were performed at room temperature using an Instron testing machine.

3. RESULTS

3.1. Microstructure of the as quenched ribbons

Two ribbons were similar, 10 and 7 mm wide and with average thickness 45 μm. The TEM microstructures and selected area electron diffraction (SAED) patterns of the ribbons are shown in Fig. 1. The characteristic broad halos were typical for the amorphous microstructure. Moreover XRD patterns also confirmed the amorphous microstructure.

3.2. Microstructure of the cold-consolidated samples

Disc shaped samples of the diameters similar to the width of the ribbons and 6–7 times thicker were achieved (Fig. 2). Optical microscopy was used to control the quality of the consolidation along the cross section perpendicular to the surfaces. It was found that the quality of the consolidation depends on the amount of strain produced by the HPT process. The samples were completely consolidated after four full turns (Fig. 2c). Samples with less number of turns showed an incomplete consolidation close to the rotation axis. The consolidation further off the center was very good (Figs. 2a, 2b). This is obviously due to the fact that the amount of strain is not only dependent on the rotation angle rather than on the distance from the center, as expected from Eq. (1). A minimal average strain, which is necessary for the full consolidation of the material is estimated according to the Eq. (1) to 4.0±0.1 at 6 GPa.

The microstructure of the consolidated samples was investigated using XRD and TEM. As shown in Fig. 3, the sample Ni-1 was crystallized in some

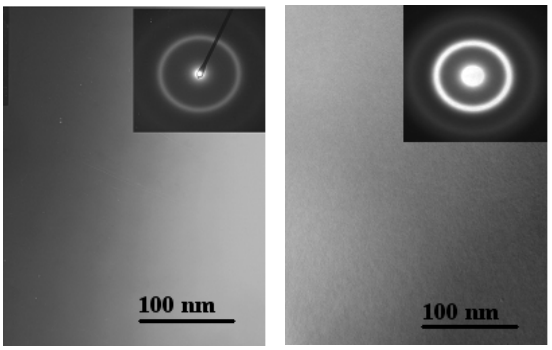

Fig. 1. TEM images (BF) and SAED patterns of as quenched ribbons: (a) $Ni_{56}Cu_2Zr_{18}Ti_{16}Al_3Si_5$, (b) $Ni_{36}Cu_{23}Zr_{18}Ti_{14}Al_5Si_4$.

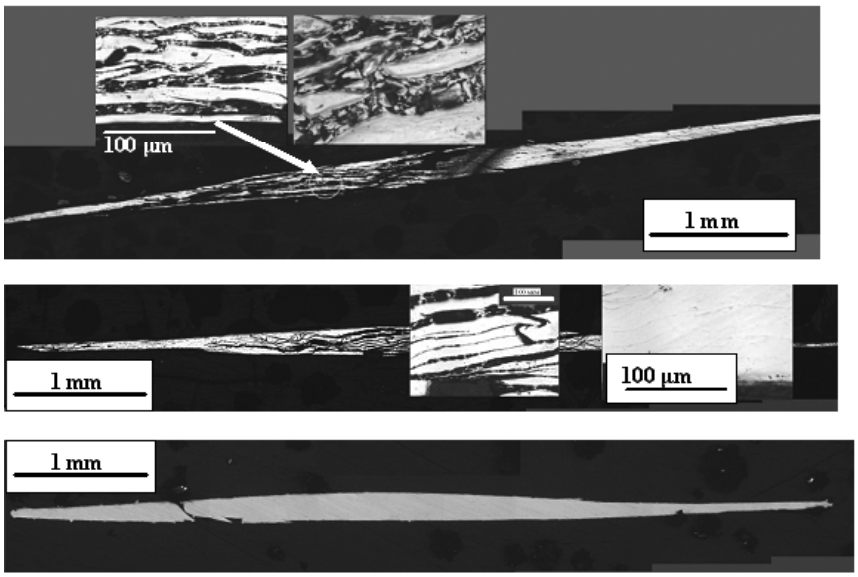

Fig. 2. $Ni_{36}Cu_{23}Zr_{18}Ti_{14}Al_5Si_4$ samples cold-consolidated by HPT at φ=2p (a), φ=4p (b), and φ=8p (c).

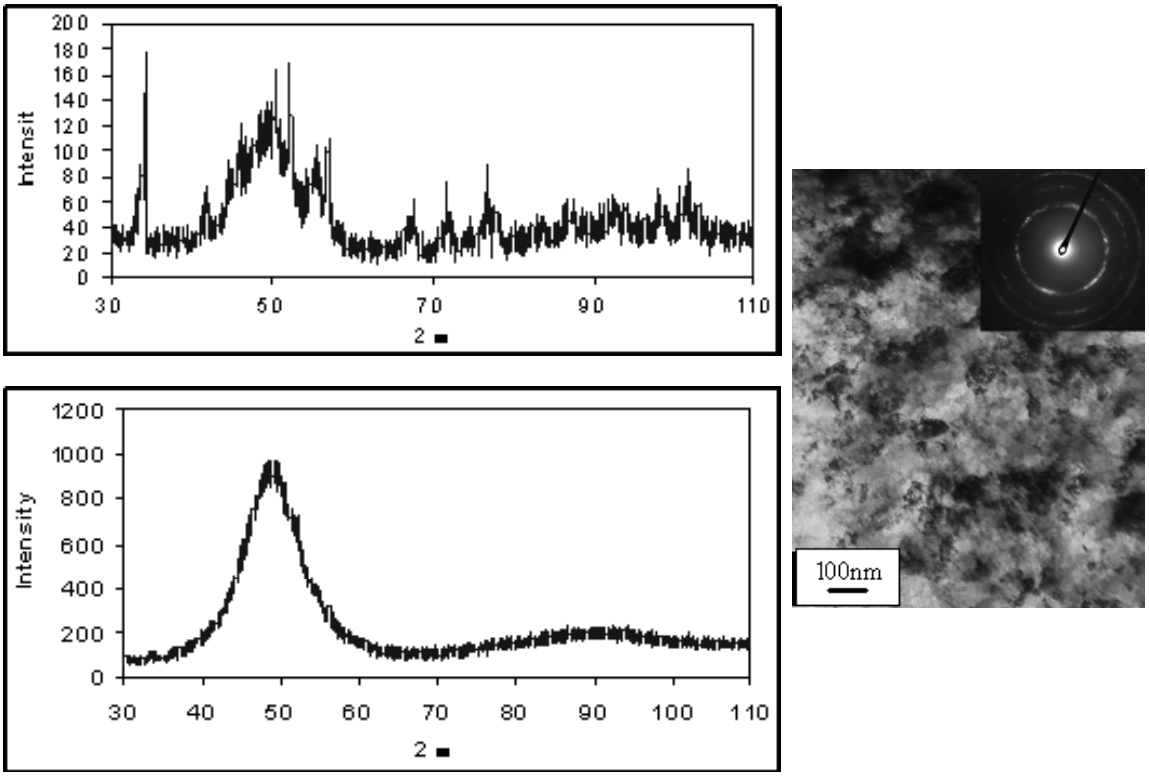

Fig. 3. XRD pattern of the consolidated ribbons $Ni_{56}Cu_2Zr_{18}Ti_{16}Al_3Si_5$ (a), and $Ni_{36}Cu_{23}Zr_{18}Ti_{14}Al_5Si_4$ (b), and TEM microstructure (c) of the cold consolidated ribbon $Ni_{56}Cu_2Zr_{18}Ti_{16}Al_3Si_5$.

part. However, the majority of the material was still amorphous, contrary to the sample Ni-2 which was fully amorphous. TEM analysis generally supported these results (Fig. 3c).

3.3. Thermal stability

To investigate the thermal stability, a DSC analysis was performed by continuous heating using a rate of 0.50 K/s. The glass transition temperature T_g (measured at the turning point) and primary crystallization temperature T_x (at the onset) for the ribbon with high Cu content were about 35K lower in comparison with the ribbon containing 2 at.% Cu. Moreover, the melting temperature (T_m) and liquidus temperature (T_l) of this alloy were lower. Both the crystallization enthalpy ΔH_c 69 J/g, and the enthalpy of fusion (ΔH_m) (3.2 kJ/mol) were slightly higher for this ribbon. All the results concerning the thermal analysis are presented in Table 1. The activation energy for crystallization (ΔE), determined by the Kissinger method (using heating rates 0.2, 0.3, 0.5, and 0.7

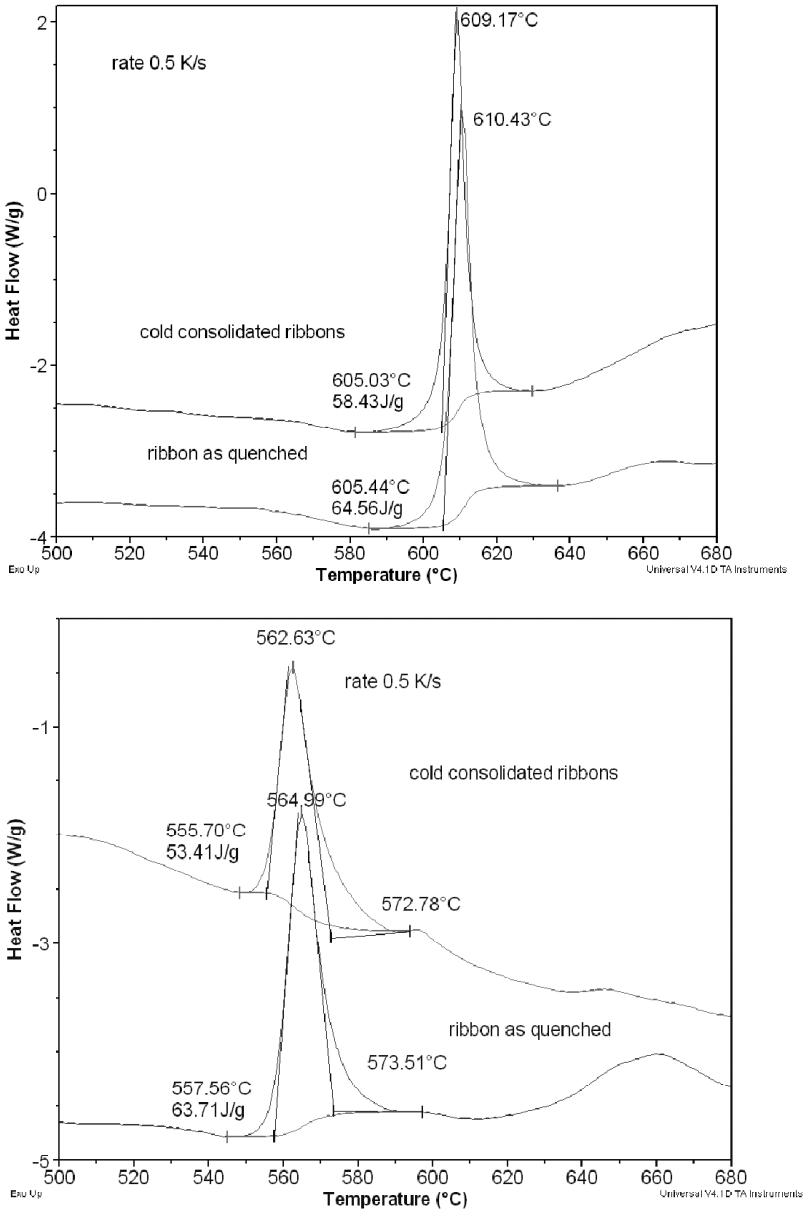

Fig. 4. The DSC curves comparing thermal stability of the ribbons and cold consolidated samples of the alloys $Ni_{56}Cu_2Zr_{18}Ti_{16}Al_3Si_5$ (a) and $Ni_{36}Cu_{23}Zr_{18}Ti_{14}Al_5Si_4$ (b).

K/s) and the difference in Gibbs free energy ΔG, which at T_g is proportional to the driving force for crystallization [9] were calculated to compare the ability for crystallization in the solid state. The ΔG was calculated with the equation $\Delta G=4\Delta H_m T^2(T_m - T)/[T_m(T + T_m)^2]$ [10] where $T = T_g$. As shown in Table 1, the calculated parameters connected to the glass forming ability are similar for both alloys but the activation energy and ΔG exhibit a higher crystallization ability for the alloy with the high Cu content.

The DSC curves comparing glass transitions and crystallization processes of the ribbons and the cold consolidated samples are shown at Fig. 4. In case of the sample $Ni_{56}Cu_2Zr_{18}Ti_{16}Al_3Si_5$ the temperatures T_x are similar and the DH_c for primary crystallization is lowered by 10% in comparison with the ribbon. In case of the sample with high Cu content the DH_c is lowered by 18% and the temperature T_x by 2K. In spite of the similarities in the primary crystallization effects, the complete crystallization may be slightly different as the secondary crystallization effects differ between cold-consolidated samples and the ribbons. More complicated changes were observed with respect to the glass transition. After HPT T_g increased by 4K for sample Ni-1, while for the sample Ni-2 with high the Cu content decreased by 7.5K, increasing undercooled liquid range from 17.6 to 23K in comparison with the ribbons.

3.4. Mechanical tests

The tensile tests and microhardness measurements showed for the ribbon Ni-1 with 2 at.% Cu a much higher strength for the hardness (8.95 GPa) and elastic modulus (111.08 GPa) than the ribbon with the high Cu content revealing a microhardness and an elastic modulus of 7.76 GPa and 97.67 GPa, respectively.

Nanohardness measurements of the cold consolidated samples showed the decrease in the hardness by 0.8–0.9 and in elastic modulus 0.7–0.8. Three point bending tests of the consolidated samples also demonstrated much higher ultimate strength in the case of Ni-1 than in Ni-2 (about 3 GPa and 1.2 GPa respectively).

3.5. Microscopic study of the fracture surfaces

SEM observations of lateral surfaces of the samples subjected to tensile and three point bending tests showed that plastic deformation occurs mainly by formation of shear bands (indicated by arrows in Figs. 5a and 5b). These bands are periodic and are similar in as quenched ribbons and consolidated samples. The fracture patterns of the as quenched ribbons are characteristic of brittle fracture and consist of clearly visible river patterns (indicated by arrows in Fig. 5c).

The fracture surfaces of cold consolidated samples are more complicated (Fig. 6). A non-uniform structure of fracture surfaces may be caused by the formation of deformation bands during the HPT process. The fracture surfaces consist of areas with dimples (marked out by circle), river patterns (marked out by triangle), and cleavage facet (marked by square). Equiaxed dimples are most likely to be formed by nucleation, growth and coalescence of microvoids. The walls of dimples represent rupture ridges, which are likely to characterize plastic deformation prior to fracture. Such a fracture surface is typical of high ductility materials. The fracture surfaces containing cleavage facet and steps of river patterns which are joined together along crack extension are characteristic of brittle fracture. SEM observations of fracture surfaces show that the consolidated sample with 2 at.% Cu revealed ductile-brittle fracture while the sample with high Cu content revealed brittle fracture. Bending tests demonstrating much higher ultimate strength in Ni-1 than in Ni-2 samples support these observations.

Table 1. Comparison of the thermal stability and GFA related parameters for the investigated amorphous alloys (heating rates for T_g and T_x: 0.5 K/s, and 0.17 K/s for melting).

	T_g [K]	T_x [K]/ ΔH_c [J/g]	ΔT [K]	ΔG [J mol^{-1}]	ΔE [kJ/mol]	T_m [K]/ΔH_m [kJ/mol]	T_l [K]	(T_g/T_l) / (T_g/T_m)	$T_x/$ $(T_g + T_l)$
$Ni_{56}Cu_2Zr_{18}$ $Ti_{13}Al_6Si_5$	852.0	864.4/ 64.7	12.4	342	506.6	1279.0/ 1.6	1294.0	0.66/0.67	0.40
$Ni_{36}Cu_{23}Zr_{18}$ $Ti_{14}A_{l5}Si_4$	813.0	830.6/ 68.7	17.6	697	449.8	1241.3/ 3.2	1262.9	0.64/0.65	0.40

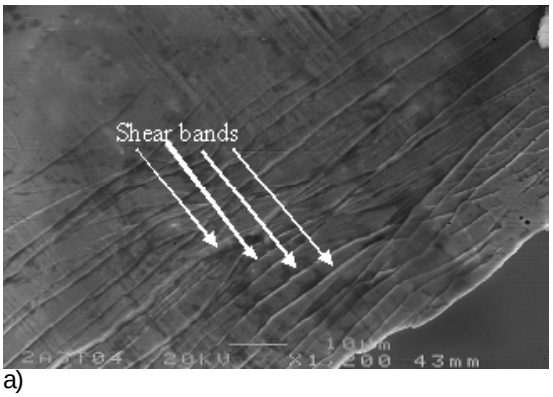

a)

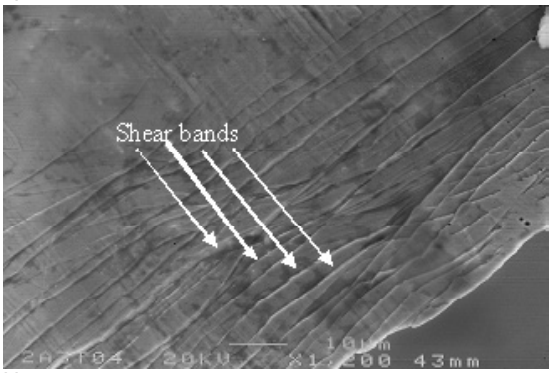

b)

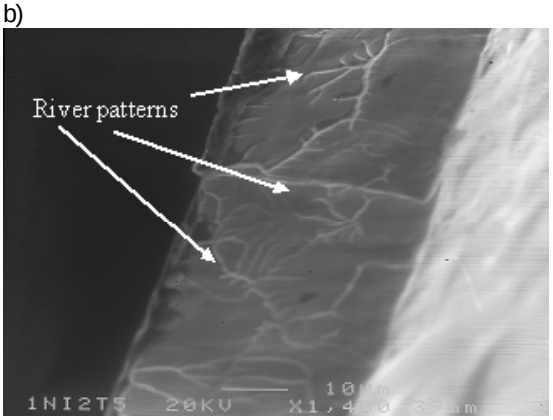

c)

Fig. 5. Lateral surfaces (a, b) and fracture pattern (c) of Ni36Cu23Zr18Ti14Al5Si4 samples after the tensile tests: (a, c) as quenched ribbons, (b) after three point bending test of consolidated sample.

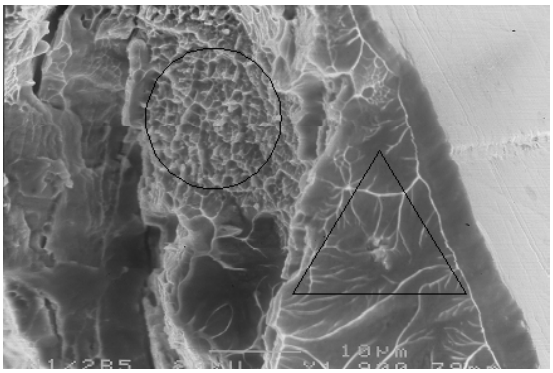

a)

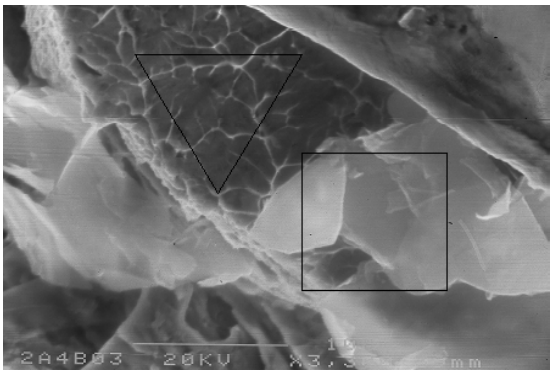

b)

Fig. 6. Fracture surfaces after three point bending tests of cold consolidated samples: (a) $Ni_{56}Cu_2Zr_{18}Ti_{16}Al_3Si_5$, (b) $Ni_{36}Cu_{23}Zr_{18}Ti_{14}Al_5Si_4$.

4. DISCUSSION

Two amorphous ribbons Ni-1 and Ni-2, which were different in composition, were subjected to a cold consolidation process by the HPT using the same parameters. The ribbon Ni-1 that contained less Cu and Al and more Zr than the ribbon Ni-2 revealed higher thermal stability with respect to the crystallization, a higher tensile strength, Young's modulus and microhardness, and was partially crystallized during the cold consolidation process. The ribbon Ni-2 preserved the amorphous state. Such results suggest that the thermal stability is not an indicator for retaining the amorphous state in the HPT process. As the temperature in the HPT process may have increased due to friction [11], the relation of the undercooled liquid temperature range to the temperature of consolidation has to be considered critical. If consolidation takes place in the ΔT range and time and temperature of the process are not enough for the isothermal nanocrystallization, the amorphous phase may be preserved. Additionally lower hardness and Young's modulus of the ribbon should support easier consolidation. These conditions were fulfilled rather by the ribbon Ni-2 than Ni-1. The DSC experiments showing changes both in the crystallization process, ΔT range and glass transition temperature of cold consolidated samples, but different for each of them, supports such a mechanism.

The results concerning the crystallization process as a result of HPT and differences in the subsequent crystallization of the cold consolidated

samples are in a good agreement with other papers [6-8]. The decrease of T_g for the sample which preserved the amorphous microstructure suggest that large shear strains may modify the amorphous structure microscopically. This was also suggested in Ref. [6]. The decrease in the hardness and elastic modulus of the cold consolidated samples may be explained by the formation of the deformation bands by the HPT process.

Generation of deformation bands by HPT was discussed in Ref. [12] in terms of free volume. According [12] the dynamic excess of free volume in amorphous materials plays an important role in decrease of plastic resistance in the shear zone that in turn leads to the strong localization of shear. In other words a local drop of viscosity takes place in the shear region that facilitates further process of plastic flow.

It is necessary to note that the most recent investigations of HPT deformed amorphous alloy revealed cycling between amorphous and crystalline states by applying successively increasing deformation [13]. The maximum amount of crystalline phase (about 80%) was detected by XRD after 0.5 turn at 4 GPa. The alloy under study was $Ti_{50}Ni_{25}Cu_{25}$ (Ni-Ti system) which is characterized by relatively low primary crystallization temperature and thermo elastic martensite transformations sensitive to shear strains. In our case we did not reveal such a cycling probably due to rather high activation energy for crystallization and primary crystallization temperature of NiZrTiSi compositions.

5. CONCLUSIONS

It was shown that under special conditions Ni- based amorphous ribbons may be cold consolidated by HPT preserving amorphous microstructure. However in most of the cases partial crystallization took place. The decisive parameters must be the subject of the further investigations. The HPT may also modify the amorphous phase properties. The decrease of mechanical properties was observed after HPT, which may be due to the formation of the deformation bands.

REFERENCES

[1] A.I. Salimon, M.F. Ashby, Y. Bréchet and A.L. Greer // *Mater. Sci. Eng. A* **375–377** (2004) 385.

[2] M. Baricco // *Advanced Engineering Materials* **9** (2007) 431.

[3] N.M. Matveeva, Yu. K. Kovneristuy, Yu. A. Bukovskiy, A.V. Shelyakov and O.V. Kostyanaya // *Russian metallurgy. Metally* **4** (1989) 171.

[4] M.D. Baró, Yu. R. Kolobov, I. A. Ovid'ko, H.-E.Schaefer, B.B. Straumal, R.Z.Valiev, I.V. Alexandrov, M. Ivanov, K. Reimann, A. B. Reizis, S. Surinach and A.P. Zhilyaev // *Rev. Adv. Mater. Sci.* **2** (2001) 1.

[5] J. Sort, D. C. Ile, A. P. Zhilyaev, A. Concustell, T. Czeppe, M. Stoica, S. Surińach, J. Eckert and M. D. Baró.// *Scripta Mater*. **50** (2004) 1221.

[6] N. Boucharat, R. Hebert, H. Rösner, R. Valiev and G. Wilde// *Scripta Mater*. **53** (2005) 823.

[7] Z.S. Kovács, P. Henits, A.P. Zhilyaev and Á. Révész // *Scripta Mater*. **54** (2006) 1733.

[8] Á. Révész, S. Hóbor, P.J. Szabó, A.P. Zhilyaev and Zs. Kovács // *Mater. Sci. Eng. A* **460-461** (2007) 459.

[9] A.-H. Cai, H. Chen, W.-K. An, J.-Y. Tan and Young-Zhou // *Mater. Sci. Eng. A* **457** (2007) 6.

[10] K.N. Lad, K.G. Raval and A. Pratap // *J. Non-Cryst. Solids* **334–335** (2004) 259.

[11] M.H. Shorshorov and A.V. Korznikov // *Materialovedenie* **6** (2002) 8.

[12] A. M. Glezer // *Bulletin of the Russian Academy of Sciences: Physics* **67, No 6** (2003) 810.

[13] G. I. Nosova, A. V. Shalimova, R. V. Sundeev, A. M. Glezer, M. N. Pankova and A. V. Shelyakov // *Kristallografiya* **54** (2009) 1111.